Incorporating a vegetation response to tidal fluctuations in salinity and water level for salt marsh representation in land surface modeling

Sophia LaFond-Hudson[1], Benjamin Sulman[1], Teri O'Meara[1], Inke Forbrich[1], and Zoe Cardon[1]

[1]Affiliation not available

June 11, 2023

Incorporating a vegetation response to tidal fluctuations in salinity and water level for salt marsh representation in land surface modeling

Authors: Sophie LaFond-Hudson, Ben Sulman, Teri O'Meara, Inke Forbrich, Zoe Cardon

Target journal: Ecological modeling or JAMES

Timeline goal:

Send to co-authors mid May

Organize code, archive code/data, revise

Resend to co-authors if needed late June

Final revisions , submit late summer 2023

Introduction

Coastal wetland ecosystems are some of the most efficient ecosystems for carbon sequestration (Mcleod et al., 2011). At the interface of land and ocean, these ecosystems are characterized by mixing of water, nutrients, and sediment from watersheds and nearshore marine waters. Productive plant communities occupy the continuum from upstream to estuary mouths, despite the dynamic gradients in physicochemical conditions. Dense vegetation slows water velocity, allowing sediment accretion that further buries organic matter produced or trapped in coastal wetlands. In addition, soils are often anoxic, slowing the decomposition of buried organic matter and allowing soil organic matter to accumulate. Land surface models (LSMs) are useful for examining carbon cycling at ecosystem scales and are critical for estimating carbon cycling in global scale Earth system model simulations. However, despite the importance of coastal wetlands in carbon storage, and their vulnerability to sea level rise, LSMs have limited representation of coastal ecosystems (O'Meara et al., 2021; Ward et al., 2020).

Plant functional types (PFTs) developed for terrestrial vegetation are inadequate for coastal wetlands because the controls on vegetation productivity differ between these ecosystems (LaFond-Hudson and Sulman, 2023). Wetland plants are sometimes exposed to soil moisture, pH, and nutrient concentrations rarely experienced by terrestrial plants, so wetland vegetation traits sometimes stray from the predictable patterns of resource tradeoffs observed in terrestrial plants (Moor et al. 2017). Models sometimes lack critical for processes in wetlands if the processes are less influential in terrestrial ecosystems. For example, in the Energy Exascale Earth System Model (E3SM)'s land surface model (ELM), vegetation productivity is limited by low soil moisture, but not by saturated soils (Oleson et al. 2013), so the model likely overestimates productivity

in coastal wetlands. The model also does not represent the impact of salt on soil water potential and photosynthesis. These missing processes lead to uncertainty in global carbon cycle projections; improving these processes will open opportunities to explore carbon cycle questions within coastal wetland ecosystems using LSMs.

Inundation decreases oxygen availability to roots under saturated soil conditions and by covering stems and leaves under flooded conditions (Colmer and Vosenek 2009). Plant adaptations to flooding can include aerenchymous tissue that transports oxygen to the root zone, increased vertical growth under flooded conditions, and floating tissues for plants adapted to permanently flooded conditions. Despite the abundant water in coastal wetlands, salinity affects plants by lowering the soil water potential outside of roots, creating challenges for water uptake. Plants may respond by limiting water uptake, or by taking up salt along with water and accumulating salt in tissues (Munns and Tester, 2008). Plants that limit water uptake must conserve water; this strategy requires lowering stomatal conductance and carbon uptake. Plants that accumulate salt have adaptations to alleviate ion toxicity within tissues, such as storage in vacuoles and production of osmolytes to maintain osmotic potential of cells. Although these adaptations are better for chronic salt exposure, these adaptations are energetically costly.

The distribution of plant communities is tightly coupled to average salinity concentrations and hydroperiod, but the physicochemical conditions of coastal wetlands are dynamic. Additionally, sea level rise, droughts, and more frequent, intense storms are likely to further vary water levels and salinity in coastal wetlands. Land surface models will be more capable of exploring carbon cycling in coastal wetlands if vegetation dynamics can be accurately simulated at the salinity and hydroperiod for which vegetation is well adapted, as well as the dynamics when vegetation is exposed to conditions for which it is poorly adapted. For example, much of the research on salt marshes in the past two decades concerns the fragility of salt marshes in the face of accelerating sea level rise. Some evidence suggests they are resilient to moderate increases in the duration of inundation via enhanced vegetation productivity that contributes to elevation gain (Kirwan et al., 2010; Morris et al., 2002). However, in some locations, marshes are eroding because local sea level rise rates are outpacing marsh elevation gain (Wasson et al., 2019). At the same time, saltwater intrusion into ecosystems that are not adapted to saline conditions can cause widespread mortality of vegetation and consequent loss of carbon stocks. Incorporating vegetation responses to salinity and inundation into LSMs is important for simulating the impacts of seasonal patterns and long-term trends in water levels and salinity on vegetation productivity in coastal ecosystems. In this paper, we describe a new capability of the DOE's Energy Exascale Earth system model (E3SM) land model (ELM) to represent vegetation responses to salinity and inundation. We show how the vegetation responses to salinity and inundation improve model accuracy in a salt marsh ecosystem. Several scenarios are then presented to demonstrate how a salt marsh might respond to systemic changes in salinity and water level, as might occur in departures from average annual precipitation.

Methods

Default land surface model description

The Exascale Energy Earth System Model (E3SM)'s land model (ELM) represents energy, water, carbon, and nutrient balances in terrestrial ecosystems, as well as processes that control the movement of energy and matter between soil layers, vegetation, and the atmosphere (Golaz et al., 2019; Lawrence et al., 2019). In the model, carbon uptake by plants is closely coupled with water uptake by roots via stomatal conductance; greater stomatal conductance is associated with both higher water and carbon uptake.

Soil water stress limits stomatal conductance through a transpiration function (Equation 1, Oleson et al. 2013). $_t$, the transpiration factor, is a value between 0 (dry) and 1 (wet). It is calculated by summing the product of w_i, a wilting factor for each soil layer, and r_i, the fraction of roots in each layer. $_t$ is multiplied by the minimum conductance to apply soil water stress.

$\beta_t = \sum_i w_i r_i$ (Equation 1)

The current study builds from salt marsh processes that have been recently implemented in ELM, includ-

ing tidal hydrology and parameterization of salt marsh graminoids (O'Meara et al., 2021). Water level is represented with a two-column approach, with one column representing a tidal channel and the other representing an adjacent, hydrologically-connected marsh. The water level in the tidal channel varies according to the tide pattern. When the water level in the tide channel is elevated above the marsh surface, water is transported laterally to the second column representing a marsh or other vegetated wetland type. In our simulations, which focus on salt marsh systems, we use the C4 grass PFT previously parameterized for *Spartina patens*based on literature values and measurements from the Global Change Research Wetland in Chesapeake Bay (O'Meara et al., 2021).

Model changes

While the previous implementation of tidal hydrology for a microtidal marsh used a sinusoidal function to represent tidal variations, modeling vegetation responses to tidal cycles across a broader range of coastal systems requires the ability to drive the model with site-specific tidal hydrology and salinity concentrations. We added the capability to read in an external forcing file containing a time series of water level heights and salinity concentrations (add github link?). The tide file may be created with measured water levels and salinity concentrations, water levels calculated from tide constituents, or hypothetical values for scenario simulations, thereby facilitating flexibility in simulating different site conditions. This approach builds the groundwork for coupling ELM to water level and salinity boundary conditions determined by ocean and river components of E3SM in future coupled simulations.

To represent the influence of salinity on vegetation growth, we used a Gaussian function (Equation 2, Li et al., 2021)

$f_i(s) = \ e^{\frac{-(s-\mu)^2}{2y^2}}$ Equation 2

In this function, s represents salinity, μ represents the salinity concentration at which maximum growth occurs (optimal salinity for a PFT), and Y represents the salinity tolerance. The function$f_i(s)$ yields a value between 0 and 1, and$f_i(s)$ is multiplied by $\mathrm{w_i r_i}$ for each layer to decrease$_t$ proportionately to the salinity concentration (Fig 1a). ELM does not represent salinity variations with depth in this study; the model is forced with a single salinity concentration applied to the entire marsh column, assuming that salinity in the marsh is equal to that in the tidal channel.

To represent the effects of flooding on vegetation growth, we used a linear function that limits carbon uptake by the proportion of vegetation that is submerged (Equation 3).

$$f_i\left(z\right) = \{ \begin{matrix} 0, & z \geq H \\ \frac{H-z}{H}, & 0 < z < H \\ 1, & z \leq 0 \end{matrix}$$ Equation 3

The inhibition of growth due to inundation,$f_i(z)$, is calculated by the plant height $H$and the surface water height z . Water levels above the plant height set $f_i(z)$ to zero, while water levels below the marsh surface set $f_i(z)$ to 1. When $0 < z < H$, the function inhibits root water uptake in proportion to the fraction of plant height that is submerged (Fig 1b). As with the salinity response,$f_i(z)$ is multiplied by the root water uptake resistance in each layer to represent the impact on root function. The improved model thus represents the soil water stress via a transpiration function that includes salinity and flood stress (Equation 4).

$\beta_t = \ \sum_i w_i \ \mathrm{r_i} \ f_i\left(s\right) f_i(z)$(Equation 4)

Model configuration, parameterization, and evaluation

ELM simulations were conducted for a temperate low marsh at the Plum Island Ecosystems Long Term Ecological Research site (PIE-LTER). The PIE-LTER low marsh is located in the Plum Island Sound in northern Massachusetts (42.7345, -70.8382) and has a humid continental climate. The site has a tidal range of 2.5-3 m and the low marsh elevation is approximately 1 m. *Spartina alterniflora* is the dominant vegetation.

The site is instrumented during the growing season with an eddy covariance tower, water level sensors, and a conductivity sensor.

Hydrological parameters for ELM (marsh level relative to tidal channel, mean water level height) were parameterized for the low marsh using observed water level data from PIE-LTER (Giblin 2019, Giblin 2022). Salinity optimum and tolerance (μ and Y) were parameterized by starting with literature values for optimal salinity for *S. alterniflora* (Vasquez et al. 2006, Maricle and Lee, 2006) and tolerance values used to model other brackish and salt marsh species with a Gaussian function (Li et al. 2021). Parameters were then adjusted until modeled gross primary production daily values (GPP) showed good agreement with measured GPP at the low marsh eddy covariance tower (Giblin and Forbrich 2022a, b, c), evaluated using root mean square error (RMSE) values. The plant functional type was set as a C4 grass and we used PFT parameters (including leaf traits, photosynthetic capacity, and growth allocation) optimized in a previous modeling study for*S. patens* in Chesapeake Bay (O'Meara et al., 2021).

We examined how observed GPP rates correlated with observed water level and salinity concentrations. To control for phenological patterns in GPP rates, we first obtained a growing season curve by averaging the noon GPP measured in 2018, 2019, and 2020 on each day followed by calculating a 60-day rolling average to smooth the three-year average. This growing season curve was then removed from the noon measurement of each year's dataset (i.e. 2018 noon GPP – seasonal average noon GPP). Pearson's correlation was used to determine the correlation of detrended GPP with water level and salinity.

We drove the model with meteorological data collected at PIE-LTER (Giblin 2019, Giblin 2020, Giblin 2021), salinity concentrations measured at xx (Giblin and Forbrich 2022a, b, c) and estimated water level using tide constituents available from NOAA Tides and Currents (https://tidesandcurrents.noaa.gov/). Data was gapfilled using linear interpolation. We assumed one salinity value for the entire soil column because ELM does not currently represent salt transport through soil layers. Model simulations were spun up using 100 years of accelerated decomposition followed by 100 years of regular spinup (Koven et al. 2013, Thornton et al. 2005). In default simulations, plant responses to salinity and inundation were inactive, representing the previous model vegetation function under site-specific meteorological, hydrological, and salinity conditions. The second set of simulations used the same meteorological, salinity, and water level forcing while including vegetation response functions to salinity and flooding. We evaluated model performance by comparing GPP from the default model simulations, improved model simulations, and measured GPP from the field site. A third set of scenarios were conducted for systematic changes in salinity by adding or subtracting a constant value (-5, +5, +10 ppt) from the 2018 salinity measurements used to force the improved model. Finally, the improved model was used to conduct scenarios for systematic changes in water level by changing the mean tide water level parameter (-10, +10, +20, +50 cm).

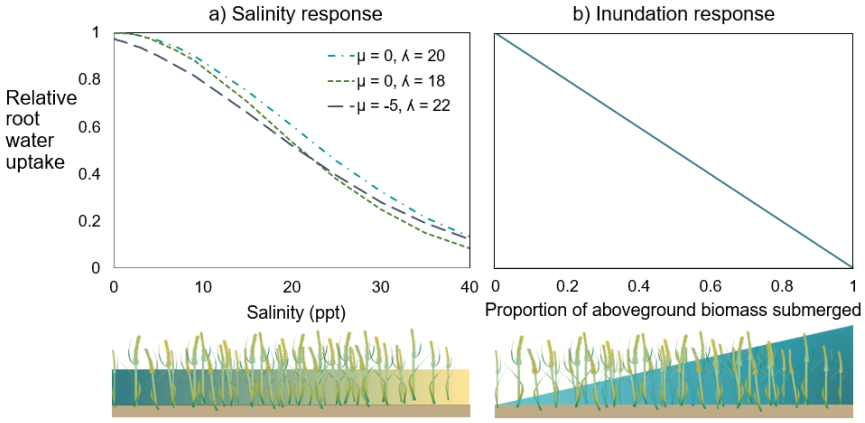

Fig. 1. The functions used to define vegetation response to (a) salinity, and (b) inundation in the model.

The salinity function requires parameterization of the optimal salinity (μ) and the salinity tolerance (Y) of each PFT. The inundation function responds linearly to the proportion of the plant submerged by surface water. Also, why didn't I just apply the same function to flooding? That would solve some problems re: flooding stimulating growth.

Results

Patterns in measured GPP

Measured carbon uptake at the low marsh shows a negative correlation with observed water level once seasonal patterns are removed (Fig. 2a,r = -0.40, 2018; Fig 2b, r = -0.30). For water levels above the marsh surface (1 m NADV88), the detrended GPP rate tended to be negative, indicating lower than average carbon uptake. Measured salinity ranged from 20-40 ppt, with annual means of 28, 29.3, and 31.1 ppt for 2018, 2019, and 2020 respectively. Salinity fluctuations did not have an obvious correlation with detrended GPP (r = 0.05, 0.02, 0.05 respectively for 2018, 2019, 2020). The literature is clear that salinity decreases growth (Munns and Tester 2008, Vasquez et al. 2006, Maricle and Lee, 2006), but the fluctuation in salinity at the low marsh may not have been wide enough to drive observable variation in GPP rates.

Model-data comparison

Several sets of salinity parameters (optimal salinity, μ, and salinity tolerance, λ, from Equation 1) were tested with the improved model to see which parameters best represented measured GPP for 2018. The simulation using (μ = 0, λ = 20) predicted the closest cumulative GPP to measurements (Fig. 3a). Modeled GPP rates with each set of parameters were compared to measured GPP rates using linear regression (Fig 3b). The simulation using (μ = 0, λ = 20) had the best agreement with data (RMSE = 5.65).

Simulations without a salinity response overestimated rates of GPP by as much as 3x (Fig. 4, 5). The inclusion of salinity and flooding functions simulated GPP values very close to measurements (Fig. 4, Fig. 5). At hourly time scales, the improved model shows decreased GPP rates during high tides (Fig. 4). The modeled water level based on NOAA tide constituents does not always represent high tide at the time it is measured in the low marsh, but the predicted water level patterns are similar to observed water levels at the site.

At annual time scales, the improved model represents the cumulative GPP within 20% of measurements (Fig. 5). The default model simulated annual productivity to be between 2700-3000 gC m^{-2}, whereas the improved model simulated annual productivity between 700-1050 gC m^{-2}. In general, the improved model tends to overestimate GPP during green-up and senescence and underestimate GPP during the middle of the growing season. The model overestimated 2018 and 2019 GPP by 10 and 19% respectively, but underestimated GPP by 21% in 2020, a year in which salinity was higher throughout the growing season, but especially during the first half.

Simulations of changing salinity and water level

We conducted two scenarios of increasing salinity (+5 ppt, +10 ppt) and one scenario of decreasing salinity (-5 ppt) to understand how sensitive the model is to changes in average annual salinity. A 5 ppt decrease in salinity (equivalent to 18% decrease relative to average salinity) over the growing season increased GPP by 39%, whereas a 5 ppt increase in salinity lowered GPP by 46% (Fig. 6). A 10 ppt salinity increase (equivalent to a 36% increase relative to average salinity) led to a 80% decrease in GPP relative to the observed salinity. The non-linear shape of the salinity response function dictates that increasing salinity would lead to a lower proportion of change in GPP (Fig. 1). However, increasing salinity also decreased plant height, which makes vegetation more susceptible to flooding effects.

We conducted one scenario in which the mean tide level decreased by 10 cm, and three scenarios in which mean tide level increased by 10 cm, 20 cm, and 50 cm (XX%, XX%, and XX% of mean high tide levels, respectively) (Fig. 7). Lowering the water level by 10 cm resulted in a 2% increase in cumulative GPP. Increasing water level by 10 cm, 20cm, and 50 cm resulted in predicted GPP declining by 2.8%, 6.3%, and

12.4%, respectively. Changing the water level did not substantially change plant height except the scenario of +50 cm water level, which decreased the maximum plant height by 12%.

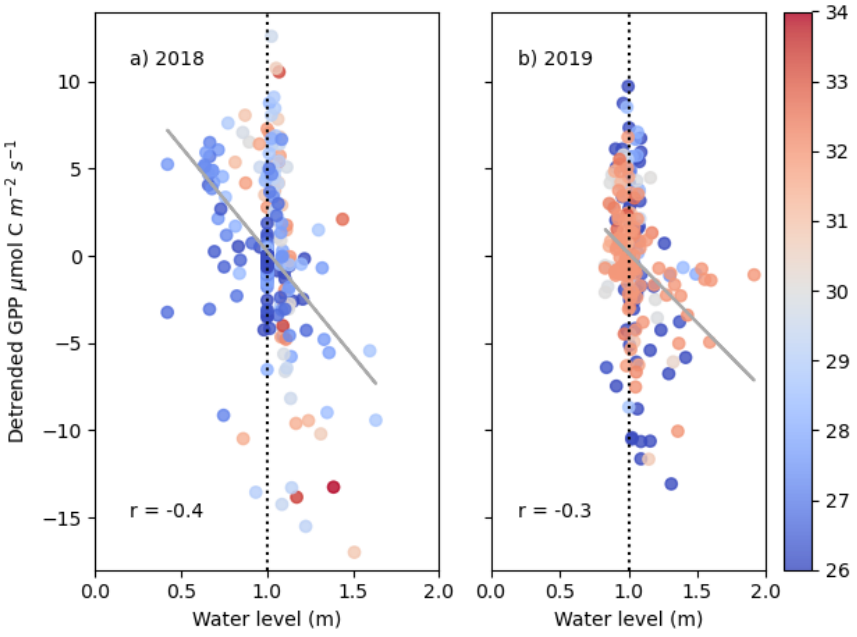

Fig. 2. Correlation between water level height (m in NAVD88) and seasonally detrended GPP rate measurements for 2018 (a) and 2019 (b). The color gradient represents the concomitant salinity concentration (ppt). The vertical dotted line indicates the elevation of the marsh soil surface (approximately 1 m). Both detrended GPP rates and water level height are from noon each day during the growing season. Positive GPP rates indicate a higher-than-average GPP rate on that day compared to an average growing season.

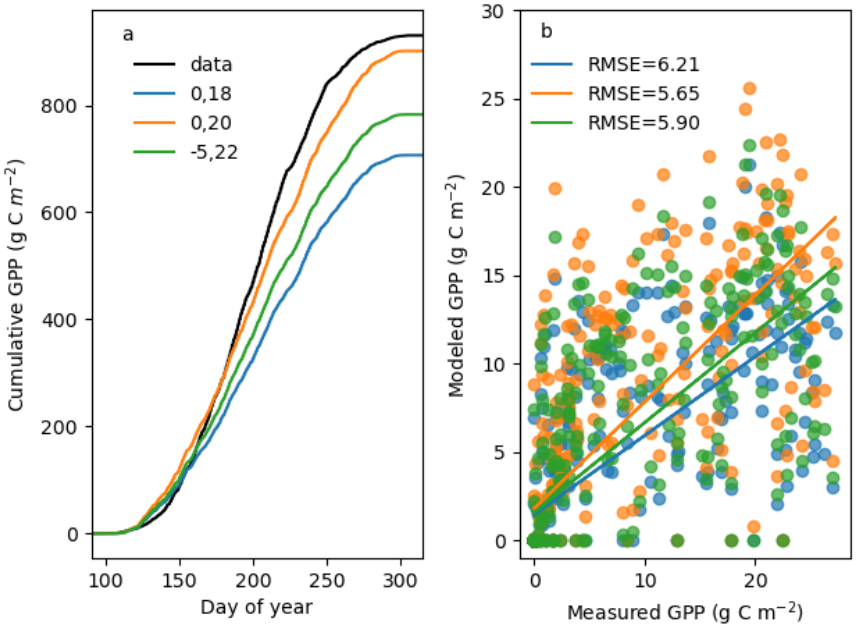

Fig 3. Parameterization of optimal salinity and salinity tolerance in the salinity response function. The cumulative GPP for 2018 was tested with three sets of parameters (optimal salinity = 0, salinity tolerance = 18, blue; optimal salinity = 0, salinity tolerance = 20, orange; and optimal salinity = -5, salinity tolerance = 22, green) and compared to measured GPP (a). The modeled daily noon GPP rates were compared to the measured daily noon GPP rates using the same three parameter sets (b).

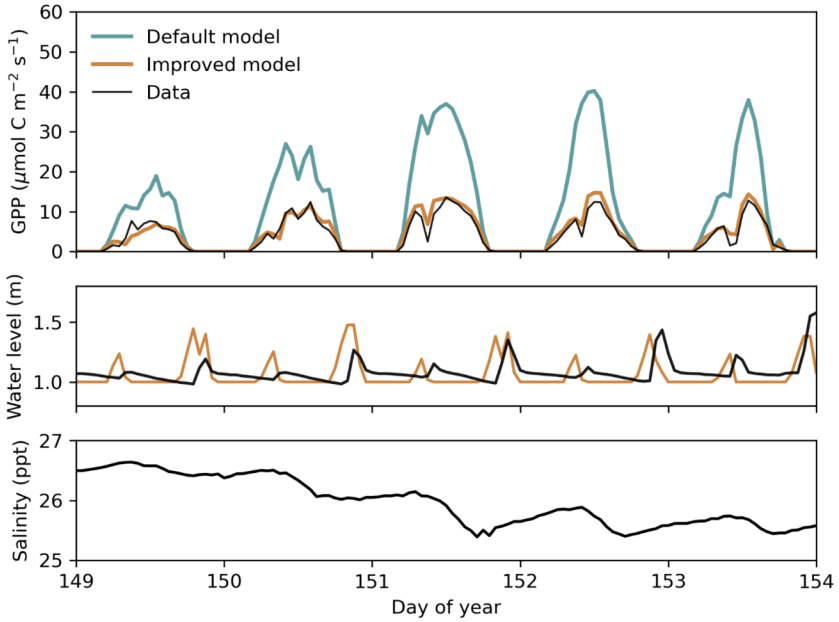

Fig. 4 Comparison of default model, improved model with salinity and flood response function, and measured gross primary productivity for 2019 (a). The improved model was forced with salinity data from the site (b). Water level in the improved model was modeled based on tidal constituents (c).

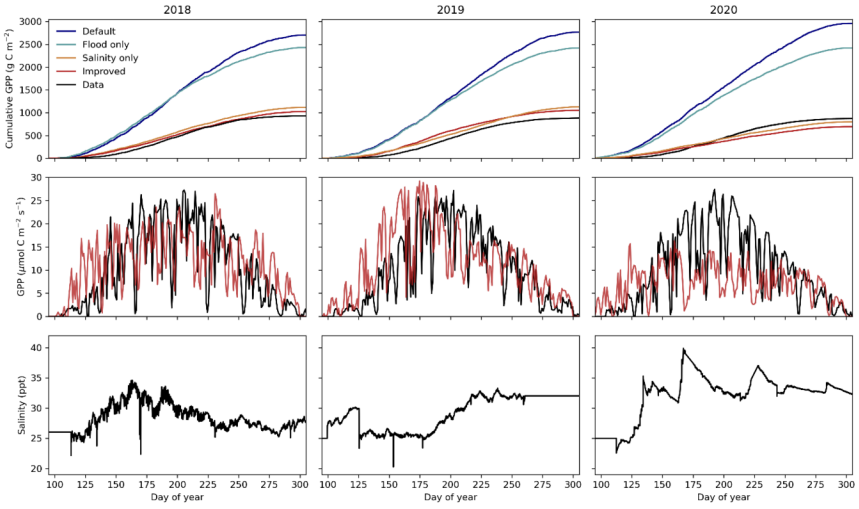

Fig. 5 Three years of model-data comparison for GPP rates and cumulative annual GPP. The bottom

row shows the site salinity measurements used to run the model simulations. This also includes the flood response.

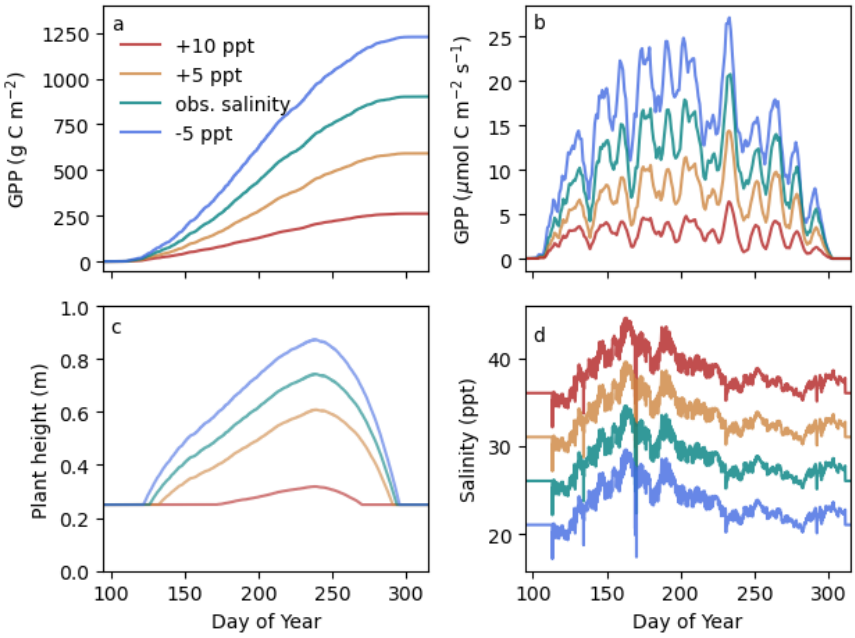

Fig 6. Scenarios showing the productivity of the low marsh may vary with salinity concentrations. The model was forced with salinity measurements from 2018 increased by 5 and 10 ppt and lowered by 5 ppt and is compared to observed (obs.) salinity.

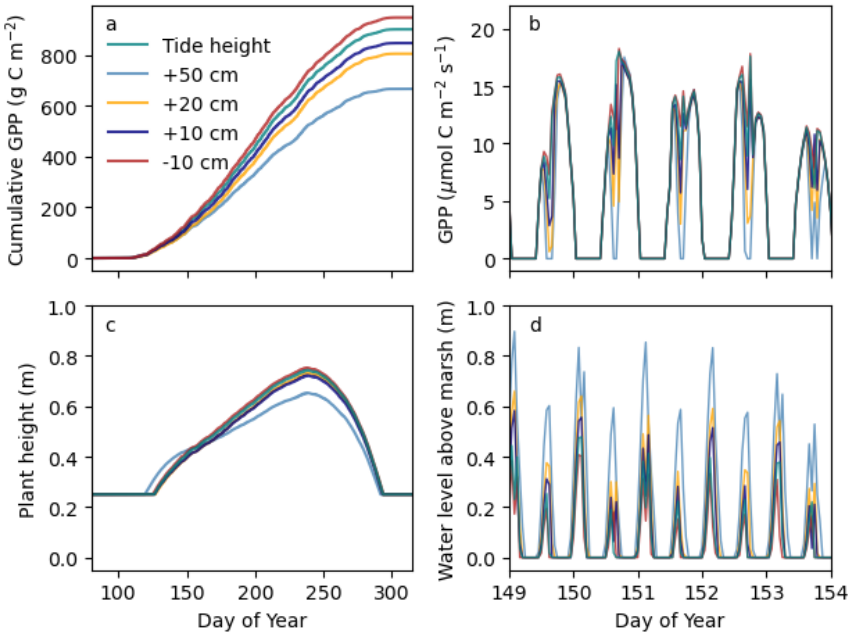

Fig 7. Simulations using the improved model to predict cumulative GPP (a), rates of GPP (b), and plant

height (c) under different water level scenarios (d).

Discussion

We modeled the effect of salinity and flooding on carbon uptake mechanistically by incorporating the relationship between salinity, flooding, and root water uptake. These modeling updates improved representation of GPP and were validated by GPP measurements taken at Plum Island Estuary. At hourly to annual time scales, modeled GPP aligned well with field observations. Incorporating salinity-induced inhibition of root water uptake brought simulations from 3x too high to near the values observed in the field. Incorporating flood-induced inhibition of carbon uptake decreased the estimated GPP by a smaller proportion compared to the salinity function, but it more accurately simulated variations over tidal cycles.

Salt marshes are well known for their strict zonation by elevation; small deviations from salinity concentration and hydroperiod result in community changes or loss of marsh habitat in lower elevations. *S. alterniflora* is a dominant species in salt marshes along North America's temperate east coast, including at the Plum Island Estuary site included in this study. Although *S. alterniflora* grows better at lower salinities, other plants compete with it in fresh and brackish conditions; *S. alterniflora* dominates salt marshes because of its tolerance to salinity concentrations and hydroperiods that kill most other species (Crain et al., 2004; Hwang and Morris, 1994). We set the optimal salinity parameter at zero to represent maximum growth in freshwater and tried several tolerance parameters to determine the value that closely simulated GPP observed in the field. Although our tolerance parameterization resulted in reasonable simulations of GPP, our model is too sensitive to salinity. Annual average salinity fluctuates by 2-3 ppt due to variation in evaporation and precipitation. Site measurements of salinity from 2020 were an average of 3 ppt higher than salinity from 2018 and measured GPP decreased by 6%, whereas the model scenarios showed an average of 5 ppt higher salinity resulted in a 40% decrease in GPP. We think the application of the Gaussian function is appropriate for mechanistic representation of salinity's limitation of carbon uptake, but the model currently lacks representation of multiple plant adaptations to salt exposure. This salinity function targets osmotic inhibition of root water uptake, but does not yet account for ways vegetation can mitigate salt exposure after uptake (Munns and Tester, 2008). plants can also take up salt and excrete it or store it in vacuoles until chronic exposure exceeds a toxicity threshold (Munns and Tester, 2008; Naidoo et al., 1992; Vasquez et al., 2006). For example, *S. alterniflora*uses solutes to adjust osmotic pressure in aboveground tissues and uses salt glands for excretion (Bradley and Morris, 1991; Naidoo et al., 1992; Vasquez et al., 2006). However, we have improved model simulations considerably from the default, and this approach has been effective in modeling biomass for other marsh species.

This model does not yet account for several important coastal wetland processes, including sediment trapping, stimulated growth, and increasing vertical accretion with moderate sea level rise. These processes are critical for understanding carbon cycling and marsh stability on decadal scales (Kirwan et al., 2010; Morris et al., 2002). Because this is the first attempt to incorporate salt marsh-specific controls on GPP in ELM, we kept our representation of flooding simple: the proportion of aboveground tissue underwater did not contribute to photosynthesis in each time step. However, this approach may be too simplistic to provide meaningful model simulations, since inundation stimulation of S. alterniflora productivity is a major control on carbon dynamics in salt marshes (Kirwan et al., 2016; Morris et al., 2013). Currently, ELM estimates plant height of grasses proportionally to LAI, which may be appropriate for approximating the impact of salinity stress on plants, but not flooding. We used Li et al.'s Gaussian approach to model vegetation response to salinity (2021), but they also used this Gaussian approach for vegetation response to flooding. In this approach, plants have an optimal flooding depth and a flooding tolerance parameter. If we adopt this approach, we will need to parameterize the salt marsh grass plant functional types for these additional flood parameters, but this information is available for *S. alterniflora*(Morris et al., 2013). In either approach, flooding above the marsh surface is addressed, but the impacts of soil waterlogging are not. Addressing soil waterlogging will likely require modeling available oxygen and other more detailed soil biogeochemistry; this work is progressing (Sulman et al. in prep?, O'Meara et al. 2021?).

Our model developments focused on improving representation of GPP in salt marshes, but to fully represent

coastal wetland carbon cycling, ELM should be able to model vegetation spanning the gradient from saline to freshwater wetlands. Our approach is flexible to model response curves of vegetation adapted to fresh or brackish conditions; even upland vegetation could be given a low salinity tolerance to model the carbon dynamics of saltwater intrusion into upland forests. However, the default model parameterization predicted GPP values 3x the measured values without the salinity response. Although individual plants may be much more productive when grown in fresh or brackish water, typically freshwater tidal wetlands are not 3x more productive than salt marshes (need to cite here). The default model therefore predicts unreasonably high values for freshwater wetland productivity, likely because the model was originally designed for upland systems and assumes that vegetation productivity is primarily limited by dry soil conditions. Thus, existing parameterization of graminoid plants likely overestimates productivity under non-water-limited conditions, so that when ELM is used to model a wetland, high soil moisture allows plants unrealistically high photosynthesis rates. As mentioned in the previous paragraph, another problem is that ELM doesn't address anoxic soil conditions, which decrease root metabolism or incur metabolic costs for flood tolerance traits (Colmer and Voesenek, 2009; Naidoo et al., 1992). Improvement of vegetation in freshwater saturated environments will be required before the model can be used to investigate carbon dynamics along a salinity gradient.

A strength of implementing coastal wetlands into ELM and our flexible approach to salinity is the potential to scale this model from point simulations to global scales. In this study, we used salinity measurements to force model simulations, combined with water levels modeled using NOAA tide pattern models. Expanding this model framework to broader scales will require estuary-scale measurements or models of coupled hydrology and salinity. These could be derived from estuary-scale measurement networks or estuary models. Simulating coastal wetland vegetation at continental to global scales within a fully coupled earth system model will require tidal patterns and salinity to be supplied by ocean or hydrological models. Current ocean models operate at resolutions too coarse to directly simulate coastal wetland tide heights and estuary salinities, but ongoing developments in high-resolution coastal models are making progress toward coupled coastal process capabilities.

Conclusion

Here, we implemented vegetation response functions to salinity and inundation to improve representation of coastal marsh ecosystems in a land surface model. In general, representing the responses of salt marsh photosynthesis to salinity and flooding via resistance to root water uptake worked well and is consistent with known plant physiological responses. Incorporating vegetation responses to salinity and inundation improved the accuracy of simulated GPP, but the updated model still overestimates productivity of freshwater wetlands. Vegetation responds to salinity and water level via several mechanisms beyond root water uptake, so our model improvements do not capture the complete vegetation response, but they provide a foundation to which additional mechanisms can be added. The stimulation of salt marsh productivity under moderate increases in inundation still needs to be addressed, as does the overestimation of productivity in freshwater marshes. Nevertheless, this work opens the door for modeling wetland C uptake along estuarine transects that include saline, brackish, and fresh marshes, or at different latitudes and tidal regimes. Additionally, salinity and flooding parameters could be applied to upland vegetation occurring at marsh edges that are much more sensitive to salinity and flooding to simulate carbon dynamics with saltwater intrusion or increasing hydroperiods.

References

Bradley, P.M., Morris, J.T., 1991. Relative Importance of Ion Exclusion, Secretion and Accumulation in Spartina alterniflora Loisel. J. Exp. Bot. 42, 1525–1532. https://doi.org/10.1093/jxb/42.12.1525

Colmer, T.D., Voesenek, L. a. C.J., 2009. Flooding tolerance: suites of plant traits in variable environments. Funct. Plant Biol. 36, 665–681. https://doi.org/10.1071/FP09144

Crain, C.M., Silliman, B.R., Bertness, S.L., Bertness, M.D., 2004. Physical and Biotic Drivers of Plant Distribution Across Estuarine Salinity Gradients. Ecology 85, 2539–2549. https://doi.org/10.1890/03-0745

Golaz, J.-C., Caldwell, P.M., Van Roekel, L.P., Petersen, M.R., Tang, Q., Wolfe, J.D., Abeshu, G., Anantharaj, V., Asay-Davis, X.S., Bader, D.C., Baldwin, S.A., Bisht, G., Bogenschutz, P.A., Branstetter, M., Brunke, M.A., Brus, S.R., Burrows, S.M., Cameron-Smith, P.J., Donahue, A.S., Deakin, M., Easter, R.C., Evans, K.J., Feng, Y., Flanner, M., Foucar, J.G., Fyke, J.G., Griffin, B.M., Hannay, C., Harrop, B.E., Hoffman, M.J., Hunke, E.C., Jacob, R.L., Jacobsen, D.W., Jeffery, N., Jones, P.W., Keen, N.D., Klein, S.A., Larson, V.E., Leung, L.R., Li, H.-Y., Lin, W., Lipscomb, W.H., Ma, P.-L., Mahajan, S., Maltrud, M.E., Mametjanov, A., McClean, J.L., McCoy, R.B., Neale, R.B., Price, S.F., Qian, Y., Rasch, P.J., Reeves Eyre, J.E.J., Riley, W.J., Ringler, T.D., Roberts, A.F., Roesler, E.L., Salinger, A.G., Shaheen, Z., Shi, X., Singh, B., Tang, J., Taylor, M.A., Thornton, P.E., Turner, A.K., Veneziani, M., Wan, H., Wang, H., Wang, S., Williams, D.N., Wolfram, P.J., Worley, P.H., Xie, S., Yang, Y., Yoon, J.-H., Zelinka, M.D., Zender, C.S., Zeng, X., Zhang, C., Zhang, K., Zhang, Y., Zheng, X., Zhou, T., Zhu, Q., 2019. The DOE E3SM Coupled Model Version 1: Overview and Evaluation at Standard Resolution. J. Adv. Model. Earth Syst. 11, 2089–2129. https://doi.org/10.1029/2018MS001603

Giblin, A. 2019. PIE LTER year 2018, meteorological data, 15 minute intervals, from the PIE LTER Marshview Farm weather station located in Newbury, MA ver 1. Environmental Data Initiative. https://doi.org/10.6073/pasta/8bd014f569ac47efe4f8fcac49cf14f7 (Accessed 2022-08-31).

Giblin, A. 2020. PIE LTER year 2019, meteorological data, 15 minute intervals, from the PIE LTER Marshview Farm weather station located in Newbury, MA. ver 1. Environmental Data Initiative. https://doi.org/10.6073/pasta/76db41052c9f8afce961fb105cc95693 (Accessed 2022-08-31).

Giblin, A. 2021. PIE LTER year 2020, meteorological data, 15 minute intervals, from the PIE LTER Marshview Farm weather station located in Newbury, MA ver 1. Environmental Data Initiative. https://doi.org/10.6073/pasta/f6985f2a9d4e9e381a08d2202caafa21 (Accessed 2022-08-31).

Giblin, A., I. Forbrich, and Plum Island Ecosystems LTER. 2022. Eddy flux measurements during 2018 from low marsh site (Spartina alterniflora) within Shad Creek catchment, Rowley, Massachusetts, PIE LTER. ver 1. Environmental Data Initiative. https://doi.org/10.6073/pasta/409a028e57d8ddc08535316dc257d083 (Accessed 2022-08-31).

Giblin, A., I. Forbrich, and Plum Island Ecosystems LTER. 2022. Eddy flux measurements during 2019 from low marsh site (Spartina alterniflora) within Shad Creek catchment, Rowley, Massachusetts, PIE LTER. ver 1. Environmental Data Initiative. https://doi.org/10.6073/pasta/1d2ec0bad48134f6924651c269ac1968 (Accessed 2022-08-31).

Giblin, A., I. Forbrich, and Plum Island Ecosystems LTER. 2022. Eddy flux measurements during 2020 from low marsh site (Spartina alterniflora) within Shad Creek catchment, Rowley, Massachusetts, PIE LTER. ver 1. Environmental Data Initiative. https://doi.org/10.6073/pasta/14354b6ca10825d7e2b043429d8d4ba9 (Accessed 2022-08-31).

Giblin, A. 2019. Marsh water table height, logging data from the Shad Creek Spartina marsh site for April-November 2018, Rowley, MA, PIE LTER. ver 1. Environmental Data Initiative. https://doi.org/10.6073/pasta/df7ab552dfdad512d91f5337e2327942 (Accessed 2022-08-31).

Giblin, A. 2021. Marsh water table height, logging data from the Shad Creek Spartina marsh site for April-November 2019, Rowley, MA, PIE LTER. ver 1. Environmental Data Initiative. https://doi.org/10.6073/pasta/605232aed464701c5b576c54f1ca7f62 (Accessed 2022-08-31).

Hwang, Y.-H., Morris, J.T., 1994. Whole-plant gas exchange responses of Spartina alterniflora (Poaceae) to a range of constant and transient salinities. Am. J. Bot. 81, 659–665. https://doi.org/10.1002/j.1537-2197.1994.tb15500.x

Kirwan, M.L., Guntenspergen, G.R., D'Alpaos, A., Morris, J.T., Mudd, S.M., Temmerman, S., 2010. Limits on the adaptability of coastal marshes to rising sea level. Geophys. Res. Lett. 37. https://doi.org/10.1029/2010GL045489

Kirwan, M.L., Temmerman, S., Skeehan, E.E., Guntenspergen, G.R., Fagherazzi, S., 2016. Overestimation of marsh vulnerability to sea level rise. Nat. Clim. Change 6, 253–260. https://doi.org/10.1038/nclimate2909

Koven, C. D., Riley, W. J., Subin, Z. M., Tang, J. Y., Torn, M. S., Collins, W. D., et al. (2013). The effect of vertically resolved soil biogeochemistry and alternate soil C and N models on C dynamics of CLM4. Biogeosciences , 10(11), 7109–7131. https://doi.org/10.5194/bg-10-7109-2013

LaFond-Hudson, S. and Sulman, B., 2023. Modeling strategies and data needs for representing coastal wetland vegetation in land surface models. *New Phytologist* , *238* (3), pp.938-951.

Lawrence, D.M., Fisher, R.A., Koven, C.D., Oleson, K.W., Swenson, S.C., Bonan, G., Collier, N., Ghimire, B., van Kampenhout, L., Kennedy, D., Kluzek, E., Lawrence, P.J., Li, F., Li, H., Lombardozzi, D., Riley, W.J., Sacks, W.J., Shi, M., Vertenstein, M., Wieder, W.R., Xu, C., Ali, A.A., Badger, A.M., Bisht, G., van den Broeke, M., Brunke, M.A., Burns, S.P., Buzan, J., Clark, M., Craig, A., Dahlin, K., Drewniak, B., Fisher, J.B., Flanner, M., Fox, A.M., Gentine, P., Hoffman, F., Keppel-Aleks, G., Knox, R., Kumar, S., Lenaerts, J., Leung, L.R., Lipscomb, W.H., Lu, Y., Pandey, A., Pelletier, J.D., Perket, J., Randerson, J.T., Ricciuto, D.M., Sanderson, B.M., Slater, A., Subin, Z.M., Tang, J., Thomas, R.Q., Val Martin, M., Zeng, X., 2019. The Community Land Model Version 5: Description of New Features, Benchmarking, and Impact of Forcing Uncertainty. J. Adv. Model. Earth Syst. 11, 4245–4287. https://doi.org/10.1029/2018MS001583

Li, Y., Yuan, L., Cao, H.-B., Tang, C.-D., Wang, X.-Y., Tian, B., Dou, S.-T., Zhang, L.-Q., Shen, J., 2021. A dynamic biomass model of emergent aquatic vegetation under different water levels and salinity. Ecol. Model. 440, 109398. https://doi.org/10.1016/j.ecolmodel.2020.109398

Mcleod, E., Chmura, G.L., Bouillon, S., Salm, R., Björk, M., Duarte, C.M., Lovelock, C.E., Schlesinger, W.H., Silliman, B.R., 2011. A blueprint for blue carbon: toward an improved understanding of the role of vegetated coastal habitats in sequestering CO2. Front. Ecol. Environ. 9, 552–560. https://doi.org/10.1890/110004

Morris, J.T., Sundareshwar, P.V., Nietch, C.T., Kjerfve, B., Cahoon, D.R., 2002. Responses of Coastal Wetlands to Rising Sea Level. Ecology 83, 2869–2877. https://doi.org/10.1890/0012-9658(2002)083[2869:ROCWTR]2.0.CO;2

Morris, J.T., Sundberg, K., Hopkinson, C.S., 2013. Salt Marsh Primary Production and Its Responses to Relative Sea Level and Nutrients in Estuaries at Plum Island, Massachusetts, and North Inlet, South Carolina, USA. Oceanography 26, 78–84.

Munns, R., Tester, M., 2008. Mechanisms of Salinity Tolerance. Annu. Rev. Plant Biol. 59, 651–681. https://doi.org/10.1146/annurev.arplant.59.032607.092911

Naidoo, G., McKee, K.L., Mendelssohn, I.A., 1992. Anatomical and Metabolic Responses to Waterlogging and Salinity in Spartina alterniflora and S. patens (Poaceae). Am. J. Bot. 79, 765–770. https://doi.org/10.2307/2444942

O'Meara, T.A., Thornton, P.E., Ricciuto, D.M., Noyce, G.L., Rich, R.L., Megonigal, J.P., 2021. Considering coasts: Adapting terrestrial models to characterize coastal wetland ecosystems. Ecol. Model. 450, 109561. https://doi.org/10.1016/j.ecolmodel.2021.109561

Thornton, P. E., & Rosenbloom, N. A. (2005). Ecosystem model spin-up: Estimating steady state conditions in a coupled terrestrial carbon and nitrogen cycle model. Ecological Modelling, 189(1-2), 25–48. https://doi.org/10.1016/j.ecolmodel.2005.04.008

Vasquez, E.A., Glenn, E.P., Guntenspergen, G.R., Brown, J.J., Nelson, S.G., 2006. Salt tolerance and osmotic adjustment of Spartina alterniflora (Poaceae) and the invasive M haplotype of Phragmites australis (Poaceae) along a salinity gradient. Am. J. Bot. 93, 1784–1790. https://doi.org/10.3732/ajb.93.12.1784

Ward, N.D., Megonigal, J.P., Bond-Lamberty, B., Bailey, V.L., Butman, D., Canuel, E.A., Diefenderfer, H., Ganju, N.K., Goñi, M.A., Graham, E.B., Hopkinson, C.S., Khangaonkar, T., Langley, J.A., McDowell, N.G., Myers-Pigg, A.N., Neumann, R.B., Osburn, C.L., Price, R.M., Rowland, J., Sengupta, A., Simard,

M., Thornton, P.E., Tzortziou, M., Vargas, R., Weisenhorn, P.B., Windham-Myers, L., 2020. Representing the function and sensitivity of coastal interfaces in Earth system models. Nat. Commun. 11, 2458. https://doi.org/10.1038/s41467-020-16236-2

Wasson, K., Ganju, N.K., Defne, Z., Endris, C., Elsey-Quirk, T., Thorne, K.M., Freeman, C.M., Guntenspergen, G., Nowacki, D.J., Raposa, K.B., 2019. Understanding tidal marsh trajectories: evaluation of multiple indicators of marsh persistence. Environ. Res. Lett. 14, 124073. https://doi.org/10.1088/1748-9326/ab5a94